The Scattering of Slow Neutrons by Paramagnetic Crystals

I. W. RUDERMAN
Department of Chemistry and Department of Physics, Columbia University, New York, New York
(Received August 1, 1949)

The paramagnetic scattering of neutrons by anhydrous crystals of manganous fluoride, manganous oxide, and α-ferric oxide was studied, using neutron transmission data obtained with the Columbia slow neutron velocity spectrometer. Details are given of the experimental arrangement, which permits measurements to be made with neutrons having wave-lengths up to 6.4A. The paramagnetic cross section, σ_{pm}, may be separated from the total cross section in regions where there are no interfering crystal diffraction effects. Large values of σ_{pm} were found for the manganous compounds, but no paramagnetic scattering by α-Fe_2O_3 was observed. The results are compared with the theoretical predictions of Halpern and Johnson. The dependence of σ_{pm} on the neutron wave-length was determined, and is compared with a theoretical form factor based on purely elastic scattering.

INTRODUCTION

IN 1936 Bloch[1] pointed out that neutrons should be scattered by ferromagnetic media because of the interaction of the magnetic moment of the neutron with the atomic magnetic field. The latter was described by a dipole distribution around and within the atom that was assumed to be unaffected by the scattering process. Schwinger[2] subsequently extended Bloch's results in a detailed quantum mechanical analysis, emphasis being placed on polarization effects in ferromagnetic substances.

In a comprehensive theoretical treatment of magnetic scattering Halpern and Johnson[3,4] introduced two new concepts: they considered in their analysis changes produced in the scatterer during the scattering process, and they proposed that magnetic scattering of neutrons be studied by means of *paramagnetic* substances. These investigators indicated that under suitable conditions the paramagnetic scattering cross section could be at least as large as, or even several-fold larger than the total nuclear scattering cross section; in such cases the experimental results might be analyzed more quantitatively and directly than ferromagnetic scattering data. The interest in magnetic scattering at that time was primarily for the purpose of gaining information about the magnetic properties of the neutron; indeed, Bloch's original intention was to provide a method for measuring the magnetic moment of the neutron.

Earlier investigators who sought to establish the existence of magnetic scattering by paramagnetic substances were handicapped by the lack of monochromatic neutron sources, meager information about neutron diffraction and scattering processes, and the difficulty of preparing pure anhydrous samples of suitable scatterers. The prior experimental evidence is based on the work of Whitaker, *et al.*[5–8] who studied the scattering of slow neutrons from a Ra-Be source by manganese and iron compounds. They compared the total cross sections obtained in transmission experiments with calculated additive nuclear cross sections, any differences being attributed to paramagnetic scattering. Using an annular ring arrangement they also studied the angular distribution of neutrons scattered in the forward direction. Only small effects were observed, and the results were in general inconclusive.

The study to be described in this paper was undertaken with the twofold objective of establishing definitely the existence of paramagnetic scattering, and seeking to utilize this effect to obtain new information about paramagnetism in solids.

THEORY

Let us consider first the simplest possible case of an isolated paramagnetic ion which scatters neutrons elastically (i.e., the neutron wave-length, λ, remains constant). Under these restricted conditions, Halpern and Johnson[4] give the paramagnetic cross section, σ_{pm}, as

$$\sigma_{pm}=[(8\pi/3)(e^2\gamma/mc^2)^2S(S+1)]F. \quad (1)$$

Here γ is the magnetic moment of the neutron in nuclear magnetons, S is the total electron spin quantum number, and F is the form factor integrated over all scattering angles. When λ is large compared with the size of the ionic magnetic domain, F approaches unity and we can evaluate the maximum value of σ_{pm} to be expected. Thus, for Mn^{++} which has five unpaired $3d$ electrons, we find $\sigma_{pm}=21.2$ barns. This is a large cross section which should be easily measurable.

A form factor for elastic scattering was approximated by Halpern in the following way. The ionic spin distribution in the initial and final states was assumed to be the same, and the spin density was taken proportional to the outer electron charge density. The latter in turn was taken to be spherically symmetrical, and was approximated by a hydrogenic wave function. It

[1] F. Bloch, Phys. Rev. **50**, 259 (1936).
[2] J. S. Schwinger, Phys. Rev. **51**, 544 (1937).
[3] O. Halpern and M. H. Johnson, Jr. Phys. Rev. **51**, 992 (1937); Phys. Rev. **52**, 52 (1937).
[4] O. Halpern and M. H. Johnson, Phys. Rev. **55**, 898 (1939).
[5] M. D. Whitaker, Phys. Rev. **52**, 384 (1937).
[6] Whitaker, Beyer, and Dunning, Phys. Rev. **54**, 771 (1938).
[7] M. D. Whitaker and W. C. Bright, Phys. Rev. **57**, 1076 (1940).
[8] M. D. Whitaker and W. C. Bright, Phys. Rev. **60**, 280 (1941).

was then possible[9] to express F as a function of $\alpha/k = 3\lambda/r_0$, where r_0 is the most probable radius of the spin distribution, and $k=1/\lambda$. F has been evaluated for various values of α/k, and the results are to be found in a recent communication.[10]

In practical cases, however, we must consider that inelastic scattering is likely to occur because of nuclear spin-electron spin, electron spin-orbit, and electron spin-spin coupling. The nuclear coupling should produce negligible effects, since the energy separations are very small compared with the neutron energy. In ionic crystals of the transition elements the crystalline field often decouples the orbital angular momentum, L, and the spin angular momentum, S, and quenches L. If the decoupling is incomplete, however, energy separations of the spin orientations comparable with kT are likely. A part of the scattering will then be inelastic. The effect of spin-spin coupling is most serious, since the energy changes due to exchange forces are probably large. The deviations of the paramagnetic susceptibility of many iron and manganese compounds from the Curie law are considered to be manifestations of spin-spin coupling. The theoretical treatment of this type of coupling is very complex, since little is known of the details of exchange forces in solids. Van Vleck[11] has extimated that in MnS, which has large spin-spin coupling, the form factor for paramagnetic scattering in the forward direction is reduced by inelastic collisions by about 75 percent and 50 percent for monochromatic liquid air and room temperature neutrons, respectively.

Fortunately, the analysis of paramagnetic scattering data may be simplified by the proper choice of scattering materials. The use of ferric and manganous compounds, in which the paramagnetic ions are in an S state, eliminates the effect of spin-orbit coupling. The effect of spin-spin coupling can then be studied by choosing a series of manganous or ferric compounds of various magnetic dilution. Our choice of compounds was influenced by the following considerations.

Paramagnetic susceptibility measurements made by many investigators[12] show that dilute solutions, or hydrates of paramagnetic substances often obey the simple Curie law, when the corresponding anhydrous crystals themselves do not. Unfortunately, aqueous hydrates and solutions are unsuitable for neutron studies because the large incoherent scattering of hydrogen would mask the paramagnetic scattering. The use of solutions would also introduce the complicating and unknown effect of solvent molecules. Only anhydrous solids were used in this study.

In Fig. 1 the closest distance, d, between Mn^{++} ions in various manganous crystals is plotted against the corresponding values of Δ in the Weiss-Curie law $\chi=C/(T+\Delta)$ for each compound. It is seen that Δ is approximately equal to zero when d is greater than 4A, but that a wide range of Δ-values exist for d smaller than 4A. It is interesting to note that there is no apparent relationship between Δ and d in the region of $d<4$A. Experimental values of Δ were used as a criterion of spin coupling. Those compounds which exhibit large values of Δ in the Weiss-Curie law can be expected to have large coupling, while those compounds which have very small values of Δ are very probably essentially free of coupling.

Our method of studying paramagnetic scattering has already been briefly outlined in a recent preliminary communication.[10] Anhydrous crystals of manganous fluoride, manganous oxide, and α-ferric oxide were chosen for study, thus providing a series of compounds of variable magnetic dilution (see Table I) with which to observe the effects of spin-spin coupling. The Columbia neutron velocity spectrometer was used to obtain transmission data for these compounds for neutron wave-lengths up to 6.4A. In the absence of paramagnetic scattering a microcrystalline sample of, say, MnO would be expected to give a cross section *vs.* time of flight curve which would be a straight $1/v$ line up to the first large diffraction peak. Data on numerous microcrystalline materials[13,14] show that there is no

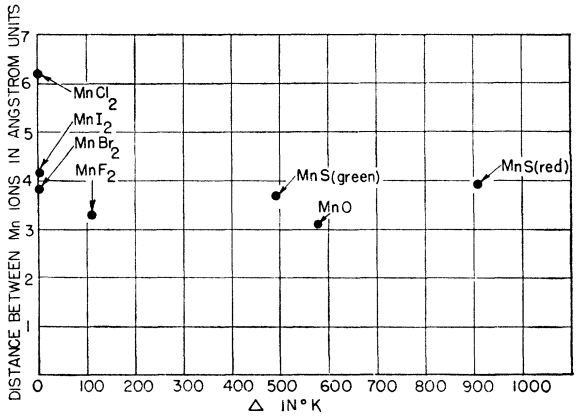

FIG. 1. The closest distance between Mn^{++} ions in several manganous compounds plotted against the corresponding values of Δ in the Weiss-Curie law for each compound. The distances were computed from x-ray data (see reference a of Table I) and the Δ-values were taken from the literature (see reference b of Table I).

[9] The integral form factor is given by Eqs. (7.40)–(7.46) in reference 4. Slight misprints occur in Eqs. (7.42), (7.43), and (7.44); for "h" wherever it appears in these equations "k" should be read.

[10] Ruderman, Havens, Jr., Taylor, and Rainwater, Phys. Rev. **75**, 895 (1949).

[11] J. H. Van Vleck, Phys. Rev. **55**, 924 (1939).

[12] See, for example, J. H. Van Vleck, *The Theory of Electric and Magnetic Susceptibilities* (Oxford University Press, London, 1932); and P. W. Selwood, *Magnetochemistry* (Interscience Publishers, Inc., New York, 1943).

[13] Sources of σ_f were as follows: Mn, this paper; O, Rainwater, Havens, Jr., Dunning, and Wu, Phys. Rev. **73**, 733 (1948); O, Melkonian, Rainwater, Havens, Jr., and Dunning, Phys. Rev. **73**, 1399 (1948); Fe, recent unpublished work in this Laboratory.

[14] See, for example, Havens, Jr., Rabi, and Rainwater, Phys. Rev. **72**, 634 (1947); Havens, Jr., Rainwater, Wu, and Dunning, Phys. Rev. **73**, 963 (1948); and Rainwater, Havens, Jr., Dunning, and Wu, Phys. Rev. **73**, 733 (1948) for curves for lead, calcite, and quartz, respectively.

TABLE I. Some important nuclear and crystallographic properties of the samples. σ_f, σ_{coh}, and σ_b are the free, coherent, and bound scattering cross sections, respectively, expressed in barns per atom for the elements and barns per molecule for the compounds. $(\sigma_b-\sigma_f)$ refers to the difference in σ due only to change in effective reduced mass. $(\sigma_b-\sigma_{coh})$ is the incoherent residual scattering cross section, assuming no lattice vibrations. λ_c is the cut-off wave-length for Bragg reflections for a microcrystalline sample, as computed from x-ray data.

Substance	Crystal class[a]	Unit cell dimensions a_0 in A	c_0 in A, or α in deg.	λ_c, in A	Δ[b] x	σ_f[c]	σ_{coh}[d]	$\sigma_b-\sigma_{coh}$	$\sigma_b-\sigma_f$
Mn						1.80	1.35	0.5	0.07
F						3.3	~4	~0	0.4
O						3.7	4.2	0	0.5
Fe						11.4	10.3	1.5	0.4
MnF_2	Tetragonal	4.885	3.295	5.46[e]	113	8.4	~8.7	0.5	0.8
MnO	Cubic	4.40		5.08	548	5.5	5.55	0.5	0.6
α-Fe_2O_3	Rhombohedral	5.414	55°17′	9.14	large[f]	33.9	33.2	2.9	2.2

[a] Crystallographic data for $MnBr_2$, $MnCl_2$, MnI_2, MnF_2, MnO, and α-Fe_2O_3 were taken from R. W. G. Wyckoff, *Crystal Structures* (Interscience Publishers, Inc., New York, 1948). The MnS data were from F. Mehmed and H. Haraldsen, Zeits. f. anorg. allgem. Chemie **235**, 193 (1938).
[b] Δ-values were from the following sources: $MnBr_2$ and MnI_2, de Haas, Schultz, and Koolhaas, Physica **7**, 57 (1940); $MnCl_2$, P. Théodoridès, Comptes Rendus **171**, 948 (1920); MnF_2, H. Bizette and B. Tsaï, Comptes Rendus **209**, 205 (1939); MnO, Bizette, Squire, and Tsaï, Comptes Rendus **207**, 449 (1938), and R. W. Tyler, Phys. Rev. **44**, 776 (1933); MnS, Bhatnagar, Prakash, and Singh, J. Ind. Chem. Soc. **16**, 313 (1939).
[c] See reference 15.
[d] See reference 16.
[e] Although the 110 plane reflects at 6.92A, the structure factor is very small and the reflection is so weak that it may be neglected.
[f] No reliable value of Δ could be found in the literature. Since α-Fe_2O_3 displays incipient ferromagnetism at 300° K, Δ is probably very large.

loss of nuclear scattering cross section until the occurrence of this first discontinuity, which is generally easily discernible. As successive diffraction peaks were passed, the coherent scattering cross section would decrease until the cut-off wave-length for Bragg reflections, λ_c, was reached. At this point all the remaining coherent scattering would disappear and the cross section would consist only of capture and incoherent scattering due to nuclear spin, lattice vibrations, lattice defects, isotope effects, etc. Suppose then that we construct a hypothetical curve consisting of a straight line which coincides with the experimentally determined curve for MnO at high energies (>1 ev), and which has the correct additive capture slope for manganese and oxygen. Let us further assume for simplicity that all the nuclear scattering cross section is retained up to λ_c for this hypothetical curve, but that beyond λ_c all coherent scattering disappears. The residual incoherent scattering cross section was estimated from the recent work of Wollan and Shull[15,16], who give values of $\sigma_{coh}=4\pi f_0^2$ where f_0 is the true bound nuclear scattering length corrected for thermal vibrations (see Table I). To obtain the effective values of σ_{coh} integrated over-all scattering angles, 0.5 barn was arbitrarily subtracted from the $4\pi f_0^2$ values to account for the loss in coherency due to thermal motion. This value of 0.5 barn is not unreasonable in the light of the work of Latham and Cassels.[17] Figures 8 and 10 show two such hypothetical curves. In those regions where there are no perturbing diffraction effects, that is for λ smaller than that corresponding to the first observable diffraction peak and for $\lambda>\lambda_c$, the difference between the experimental and the hypothetical curve was taken to be σ_{pm}.

The crystal size of the sample is significant. A large single crystal has the advantage of quickly becoming almost transparent with decreasing neutron energy.[14] Approximate values of σ_{pm} (neglecting the small amount of coherent scattering which still remains) can therefore be obtained for a considerable range of λ smaller than λ_c. However, no determinations of σ_{pm} can be made at short wave-lengths (0 to ~3A). For a microcrystalline sample, individual crystals should not be so small (~1μ or less) that appreciable small angle scattering occurs,[18] nor so large that the sample becomes transparent.

EXPERIMENTAL

1. Neutron Spectrometer

The Columbia slow neutron spectrometer has already been described in detail by Rainwater and Havens.[19–21] The spectrometer consists essentially of the 36-in. cyclotron, timing circuits for modulating the arc and operating the detection chain, a slow neutron paraffin "source" slab, collimation and shielding, and BF_3 proportional counters for detection. The details of the collimating system as modified for the experiments described in this paper are given in Fig. 2. The 5-meter source-to-detector distance was used for measurements

[15] The σ_{coh}-values for the elements (corrected for thermal motion) were kindly supplied by Dr. C. G. Shull, and represent his most recent results. These values were taken to be additive in computing σ_{coh} for the compounds.
[16] See for example E. O. Wollan and C. G. Shull, Phys. Rev. **73**, 830 (1948); Shull, Wollan, Morton, and Davidson, Phys. Rev. **73**, 842 (1948).
[17] R. Latham and J. M. Cassels, Nature **161**, 282 (1948); J. M. Cassels and R. Latham, Phys. Rev. **74**, 103 (1948); J. M. Cassels, private communication, September 21, 1948.
[18] Krueger, Meneghetti, Ringo, and Winsberg, Phys. Rev. **75**, 1098 (1949).
[19] J. Rainwater and W. W. Havens, Jr. Phys. Rev. **70**, 136 (1946).
[20] W. W. Havens, Jr., and J. Rainwater, Phys. Rev. **70**, 154 (1946).
[21] Rainwater, Havens, Jr., Wu, and Dunning, Phys. Rev. **71**, 65 (1947).

with neutrons having wave-lengths greater than 3A, and the regular 6-meter collimation for shorter wave-lengths.

Deuterons, produced in the cyclotron chamber by modulating the accelerating potential on the ion source have an energy of 8 Mev when they strike the beryllium target. The fundamental timing for the circuits which control the cyclotron and detector is now provided by a 1-megacycle crystal-controlled oscillator. This provides cyclotron and detector on-times of 2, 4, 8$\cdots$512 or 1024 μsec., and cyclotron repeat times of 1024, 2048$\cdots$16384, or 32768 μsec.

The true resolution function is rather complex, but has always been found to be roughly triangular in shape. The width of the triangular base for all the measurements reported in this paper lies between 2 and 3 times the timing spacing between adjacent experimental points shown on the curves.

A "thin" neutron source, consisting of a 24.2-cm $\times$24.2-cm$\times$3.8-cm paraffin block covered on all sides by $\frac{1}{4}$-in. plywood, was used for neutron wave-lengths up to 1.25A. The back face (away from the collimating system) of the paraffin is mixed with boron carbide for a depth of 0.6 cm to keep out stray slow neutrons. For longer wave-lengths a "thick" source was used in order to obtain greater slow neutron intensity. The thick source is 22.8 cm$\times$22.8 cm$\times$6.5 cm and is covered by $\frac{1}{4}$-in plywood on the faces and $\frac{1}{2}$-in. plywood on the sides; in addition, the back face is covered with a 0.022-in. thick cadmium sheet.

2. Method of Making Transmission Measurements

Transmission measurements were made as follows. The sample was placed in the proper place in one collimated channel, and a "dummy" consisting of an aluminum disk of thickness equal to the total wall thickness of the sample holder was placed in the corresponding position in the second channel. After a definite number of neutron counts from a monitor fission counter placed in the cyclotron enclosure, the counts recorded by the registers for each channel were noted. The sample and dummy were then interchanged in position, and the registers read after another equal number of monitor counts. This constitutes a complete "cycle." Sufficient cycles were run to obtain the desired statistical ac curacy.

The total number of counts for a detection interval taken over all the cycles with the sample in the beam ("in" position), divided by the corresponding total number of counts with the dummy in the beam ("out" position) gives the transmission for this interval. Transmission values obtained in this way for each channel were averaged to give the final value. The cross section, σ, was obtained from the transmission, T, by the relation $T=e^{-n\sigma}$, where n represents the atoms or molecules per cm^2 in the sample. The use of two channels tends to minimize errors due to changes in neutron flux and counter efficiency. To take full advantage of this feature, the number of monitor counts per cycle was kept as low as was compatible with efficient operation and good statistical accuracy.

The background counting rate was determined at least once or twice during each run by substituting 3-in. thick disks of a boron carbide-paraffin mixture for the sample and dummy in each channel. The background counts were in all cases either zero or negligibly small. This test shows that the counters are well-shielded and do not count spuriously, but it gives no indication of the stray neutron effect to be described shortly.

3. Use of "Standard Filters"

Early in this work it was observed that the two channels gave appreciably different transmissions for

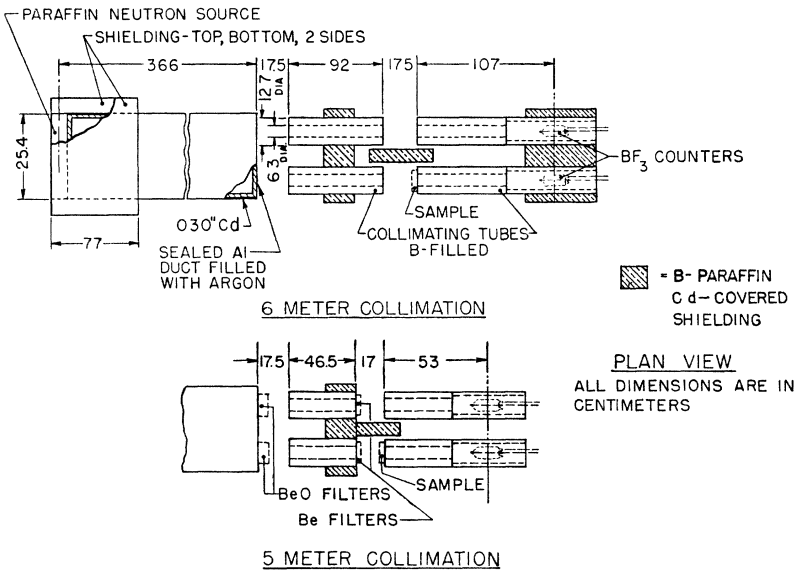

FIG. 2. Details of the collimating system for 5- and 6-meter source-to-detector distances. Not shown for clarity is the additional shielding which surrounds completely the collimating tubes and counters.

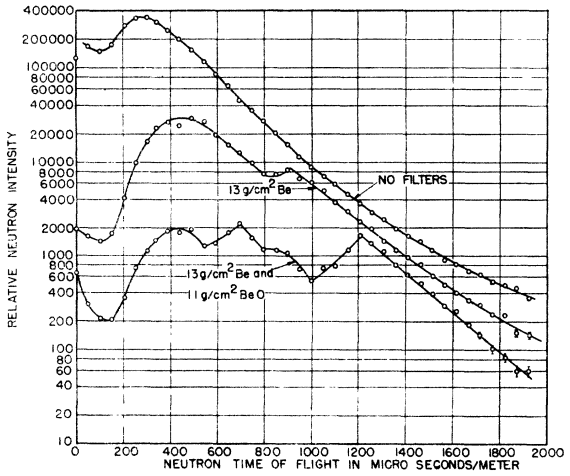

FIG. 3. The effect on the neutron distribution from the source of beryllium and beryllium oxide filters.

the same sample, and that the general reproducibility of results, particularly in the high energy region, over long periods of time was not entirely satisfactory. A rate dependence of the counters was considered to be responsible for this, and "standard filters" whose design and operation are fully described elsewhere,[22] were found to eliminate these discrepancies. These standard filters were used in all our transmission experiments for neutron wave-lengths less than 2.6A.

There are indications that the counter rate dependence has both an instantaneous and a delayed component. The latter arises from the neutron flux which causes pulses in the BF_3 counters and allied circuits during those intervals of time when the source is emitting neutrons but the detection chain is not activated. For $\lambda > 2.6$A standard filters were not used because it was believed that the great reduction in thermal neutron flux resulting from the use of Be and BeO filters (see Fig. 3 and the discussion on stray neutrons which follows) would eliminate the delayed effect, while the normal reduction of slow neutron intensity because of the Maxwellian distribution would markedly diminish the instantaneous effect. The poor neutron intensity at long wave-lengths also discourages the use of any apparatus which reduces this intensity. Recent experiments have shown that standard filters are indeed unnecessary for $\lambda > 2.6$A.

4. Effects and Possible Sources of Stray Neutrons

From preliminary experiments it was found that for neutron wave-lengths greater than 4.4A, the cross section of manganous fluoride ceased to increase with increasing wave-length (as it should do because of the manganese capture slope), but instead flattened off and started to decrease. This effect was interpreted as being due to stray neutrons. It was apparent that the Be filters, which were used for these measurements in order to discriminate against stray neutrons having energies greater than ~0.01 ev, were inadequate. It was decided to examine this difficulty in some detail.

Three main sources of stray neutrons were considered:

(1) Faster thermal neutrons, emitted by the source and reflected from the walls of the cyclotron enclosure, might strike air molecules in the open space inside the enclosure between the source and the collimating tubes (i.e., the space now occupied by the aluminum duct shown in Fig. 2) and be scattered into the neutron beam. These neutrons would reach the detector at the same time as the "regular" group of slow neutrons

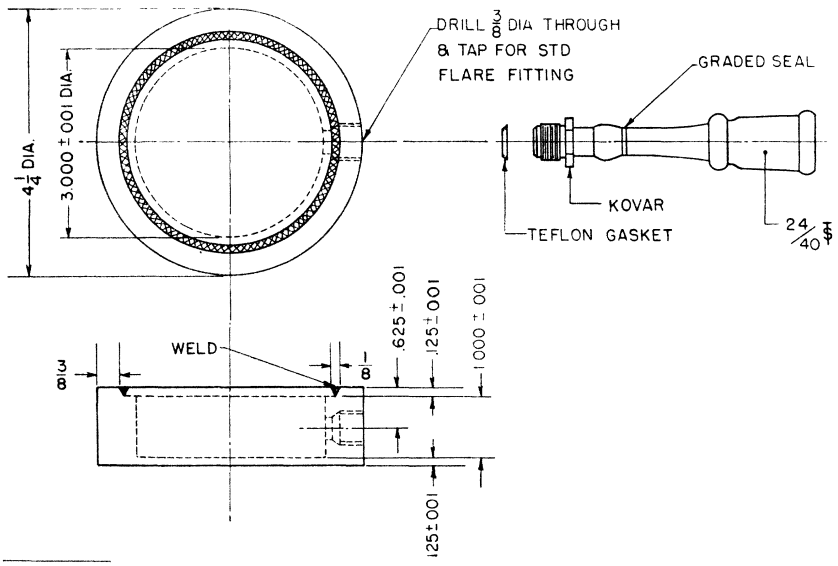

FIG. 4. Details of the aluminum alloy sample holders.

[22] E. Melkonian, Ph.D. thesis, Columbia University, 1949, to be submitted for publication.

which go directly from the source to the detector. Since they would have, in general, a larger straightened out path length, they would have a greater average velocity or energy than that associated with any given timing interval. The *measured* value of the transmission of the sample for a given timing interval would then correspond to a weighted average of the transmission due to the regular group and to these faster in-scattered neutrons. The observed cross section would hence be lower than the true cross section for the given timing.

(2) A small residual neutron production in the vicinity of the arc source, when the latter is supposedly not emitting, would produce a background of neutrons with an essentially Maxwellian distribution. Since the thermal peak is at approximately 1.1A, the weighted contribution of these neutrons would depend upon the transmission of the sample at 1.1A. For manganese and iron compounds, which have a considerable $1/v$ slope, the transmission at 1.1A is much higher than it is at wave-lengths greater than 4.4A. The observed transmission would therefore be higher than it should be, and lower cross sections would be obtained.

(3) The regular group of neutrons reaching the detector in the timing interval t_0 to $t_0+\Delta t_0$ move in a straight line from the source to detector with constant velocity v_0 to $v_0-\Delta v_0$. If small angle inelastic scattering could occur, there would be an additional contribution to the interval t_0 to $t_0+\Delta t_0$ due to neutrons having a velocity $v_1>v_0$ from source to sample and velocity $v_2<v_0$ (after inelastic scattering) from the sample to the detector. In order to reach the detector in the given timing interval, the *time average* value of the velocity must lie in the range v_0 to $v_0-\Delta v_0$. Since the relative number of neutrons $N(v)$ detected in any velocity interval decreases $\sim v^6$ as v is decreased in the low energy range, there will be very many more faster neutrons reaching the sample than neutrons of the given velocity. If any appreciable fraction could be inelastically scattered (as described above) the in count would be considerably increased. However this effect will probably not be serious for a number of reasons.

a. Since the sample-to-detector distance is only one-tenth the source-to-detector distance, the ratio v_0/v_2 must be much larger than the ratio v_1/v_0 (in the energy region of interest) in order to give the proper time average velocity. Since the neutron energy after a collision tends to be restored towards kT, the probability of finding a very low velocity v_2 after collision must be exceedingly small.

b. Properly we should also consider hyperelastic processes where $v_2>v_0$ after collision. This again should be unimportant because $N(v)$ decreases rapidly as v decreases so there are relatively few neutrons with $v_1<v_0$. Both of these processes (a and b) which *add* to the number of neutrons reaching the detector in the given detection interval, will be largely counterbalanced by the loss due to the small angle inelastic scattering of neutrons with velocity v_0 to $v_0-\Delta v_0$ in the source-to-sample region. That is, an inelastic process merely shifts a neutron of given initial velocity from its regular detection interval to a different one, and the losses and gains will tend to balance for any given detection interval.

c. Since the detector subtends but a small solid angle at the sample, the differential inelastic cross section would have to be quite large to introduce any measurable error. That the total inelastic cross section is small, however, is shown by the work of Weinstock[23] and Latham and Cassels[17] as well as by the small residual cross sections obtained in this Laboratory for various crystalline solids at $\lambda>\lambda_c$.[23a]

In order to reduce any existing background of neutrons scattered into the beam by air molecules, all of

TABLE II. Source, sample and detector geometry.

	Solid angle (in steradians) subtended at:	By source 5 meters	By source 6 meters	By detector 5 meters	By detector 6 meters
Infinite source	Sample	0.0081	0.0027	0.0069	0.0017
	Detector	0.0023	0.00066		
24.2 cm×	Sample	0.0030	0.0024		
24.2 cm source	Detector	0.0023	0.00066		

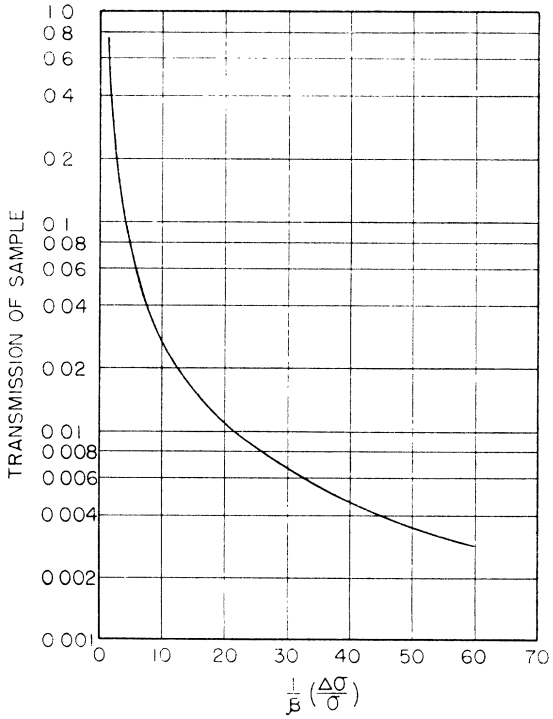

FIG. 5. The relative error in cross section due to small angle scattering into the detector as a function of the transmission of the sample. The total cross section is assumed to be due only to scattering processes, which are spherically symmetrical.

[23] R. Weinstock, Phys. Rev. **65**, 1 (1944).
[23a] P. J. Bendt and I. W. Ruderman, Phys. Rev. **76**, 463 (1949).

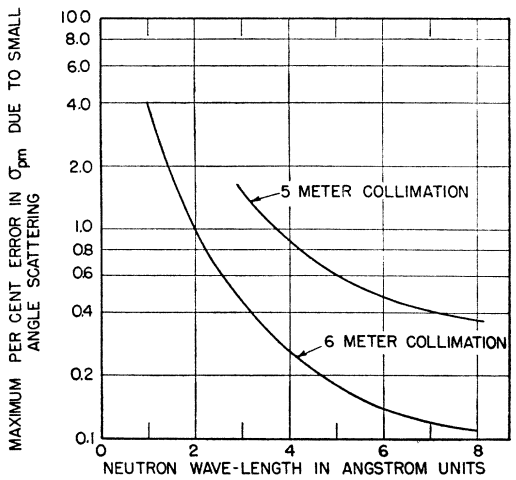

FIG. 6. The maximum percent error in σ_{pm} due to small angle scattering into the detector as a function of neutron wavelength for a typical paramagnetic sample, taking into account non-spherically symmetrical scattering.

the neutron path open to the air in the cyclotron enclosure was replaced by a cadmium-lined, argon-filled duraluminum duct (Fig. 2). The heavier and bulkier construction which an evacuated duct would have entailed mitigated against its use, in spite of its obvious superiority. The duct, constructed in three separate sections for flexibility in handling, was made of 3/32-in. duraluminum sheet. Each section was completely sealed and air-tight except for a small tapped hole at each end. These holes were used to flush the duct with argon until essentially all the air was replaced with argon at atmospheric pressure, after which the holes were sealed with plugs. The sides of each section were covered with 0.030-in. cadmium sheet. Argon was chosen as the filling gas because of its low total and scattering cross sections. Since 366 cm of air has a transmission at 5A of 0.73, while the same thickness of argon has a transmission of 0.97, approximately a 33 percent increase in neutron intensity at 5A is to be expected. Such an improvement in intensity was indeed observed when this new collimating duct was put into use.

In order to reduce further the stray neutron background, all measurements at $\lambda > 2.6$A were made with neutrons filtered by 13 g/cm^2 of Be and 6–11 g/cm^2 of BeO. The effectiveness of Be and BeO in reducing the neutron intensity below about 3.5A is shown in Fig. 3.

In addition to the corrective measures already described, measurements in the neighborhood of 6A were corrected for background neutrons as follows. Using neutron burst repeat times of 32768 μsec., the neutron intensity was determined in the region from 16384 to 32768 μsec. Any neutrons that were counted were considered to be due to background, since the desirable neutron intensity should be immeasureably small in this region. The maximum corrections were of the order of 1 percent, and were significant only when the in count was very small. The background observed in this manner is considered to be due to a (very small) continuous emission of neutrons from the cyclotron, resulting from a weak deuteron production near the ion source when the arc is supposedly turned off.

5. Preparation of Samples

Manganous fluoride: Reagent grade $MnCO_3$ was added to a pure 48 percent HF solution contained in a polyfluorochloroethylene beaker. The precipitate which formed was given time to settle, and the supernatent liquid was decanted. The precipitate was washed several times with pure ethanol, and then dried in air with infra-red lamps. The dry powder was fused in a boron-free graphite crucible at 950°C in an atmosphere of HF. The clear, orange-violet crystalline mass was crushed, and a uniform batch of 0.5-mm crystals was obtained by sieving. The calculated Mn content of MnF_2 is 59.11 percent; found by analysis, 59.03±0.03 percent.

Manganous oxide: Reagent grade $MnSO_4 \cdot 5H_2O$ was dried at 130°, and then heated in air at 1100°C for several days. The brown-black Mn_3O_4 was ground to a fine powder, which was reduced to MnO by heating it at 1100°C in a stream of hydrogen containing a trace of HCl.[24,25] The product was cooled to room temperature in a stream of pure hydrogen, and was thoroughly degassed in a high vacuum system with the aid of infra-red heating (75–130°C). The final product consisted of fine, bright green crystals. The calculated Mn content of MnO is 77.44 percent; found by analysis, 77.42±0.01 percent.

α-Ferric oxide: A large, essentially single, natural crystal of hematite in the shape of a plate 3.65-cm thick was used. The two flat faces of the crystal are very parallel, and are perpendicular to the three-fold axis of symmetry. The calculated Fe content of Fe_2O_3 is 69.94 percent; found by analysis, 69.80±0.08 percent.

Manganese: Electrolytic manganese of 99.9+ percent purity was pulverized, and a uniform quantity of 0.5 to 1-mm particles was obtained by sieving. The sample was dehydrogenated by heating at 400° in vacuum for several hours.

Spectrographic analysis of each of the samples showed the absence of any significant quantity of B, Cd, Co, Cu, Cr, Ni, or Pt.

6. Packing of Samples

The sample holders, shown in Fig. 4, were made of 17ST aluminum alloy. To avoid distortion of the thin, flat walls during welding, both walls were machined $\frac{1}{8}$ in. thicker than desired; after welding the walls were turned down to the proper thickness.

The dry sample was added in small portions to the sample holder through the tapered glass neck, the holder being tapped repeatedly after each addition in order to

[24] R. W. Millar, J. Am. Chem. Soc. **50**, 1875 (1928).
[25] H. S.-C. Deville, Comptes Rendus **53**, 199 (1861).

provide good packing of the sample. When the holder was filled to the top of the Kovar seal, and tapping produced no further change in level, the holder was connected to a high vacuum system. After thorough degasing, the system was filled with dry helium and the holder was sealed off just above the graded seal.

DISCUSSION OF ERRORS

1. Small angle scattering

This error is introduced because some neutrons scattered at small angles are counted by the detector. Moreover, since with the geometry used the sample sees more of the source than does the detector, the in-count neutron flux at the sample is greater than the out-count neutron flux at the detector; the error is consequently magnified. For simplicity, a sample having *no capture* is assumed.

Case I: 6 meter neutron path. Since the neutron source is of such limited size that not all parts of the sample can see the full solid angle of the source permitted by the collimating system, the relative geometry of the source, sample, and detector has been calculated on two bases (Table II). For an infinite source the solid angles subtended at the sample and detector by the source would be defined by the 6.3-cm collimating tube, while for the actual source used these solid angles may be considered to be fixed by the area of the source. As will become apparent shortly, the former basis leads to an upper limit for the error under consideration, and the latter to a minimum error. The true error is somewhere between these limits. It is assumed throughout that the source emits neutrons uniformly over its entire surface; localization of emission at the center of the source would tend to reduce the in-scattering error.

Let the incident neutron flux at the detector in the out position be N. Then the incident flux at the sample position in the in count is, for the case of an infinite source, equal to $(0.0027/0.00066)N=4.1\ N$, of which $3.1N$ cannot be seen by the detector unless it is scattered at very small angles into the detector by the sample. Of the remaining N flux, $(1-T)N$ will be scattered, and a fraction of this will take place at such small angles that it will be seen by the detector. If the scattering is spherically symmetrical, then the total extra in-scattered flux is

$$\frac{(0.0017)}{4\pi}4.1N(1-T)=0.0006N(1-T).$$

The absolute error in T is given by

$$\Delta T=0.0006(1-T)=\beta(1-T),$$

and the relative error in cross section is

$$\Delta\sigma/\sigma=\beta(1-T)/T\ \ln T. \qquad (2)$$

The relative error in cross section thus depends upon the transmission of the sample, and this dependence is shown in Fig. 5. The error increases rapidly for transmissions lower than about 5 percent. It should be noted, however, that an observed transmission of say 14 percent in the case of manganous fluoride corresponds to a transmission of about 61 percent if the manganese capture is corrected for, and only scattering processes are considered. With $T=0.61$ and $\beta=0.0006$ the upper limit for $\Delta\sigma_{pm}/\sigma_{pm}$ is less than 0.1 percent.

The derivation of the in-scattering error given above

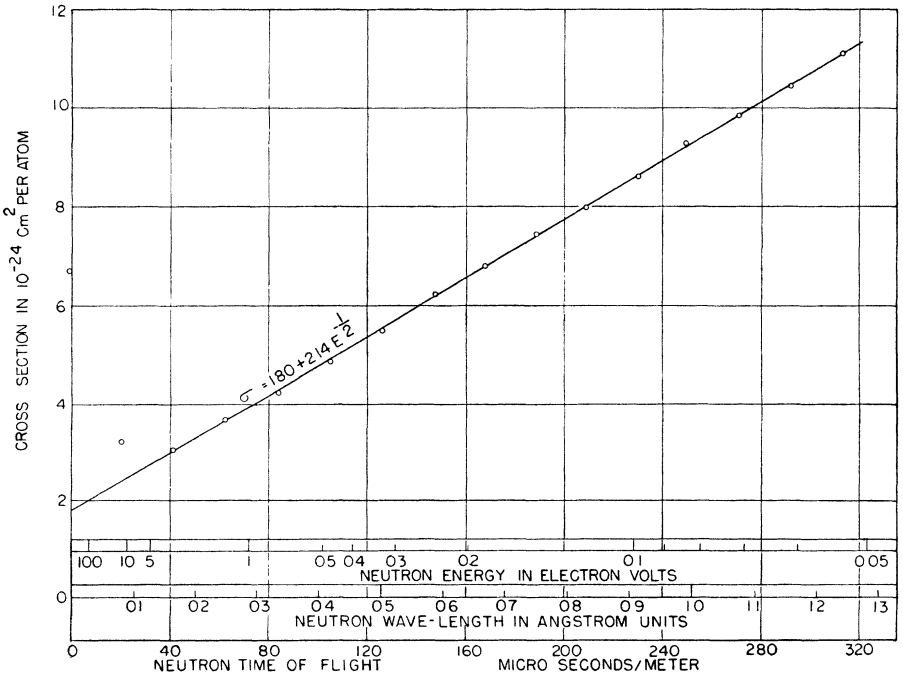

FIG. 7. The observed total cross section of 16.92 g/cm² of manganese as a function of neutron energy. The best $1/v$ line is $\sigma=1.80+2.14E^{-\frac{1}{2}}$.

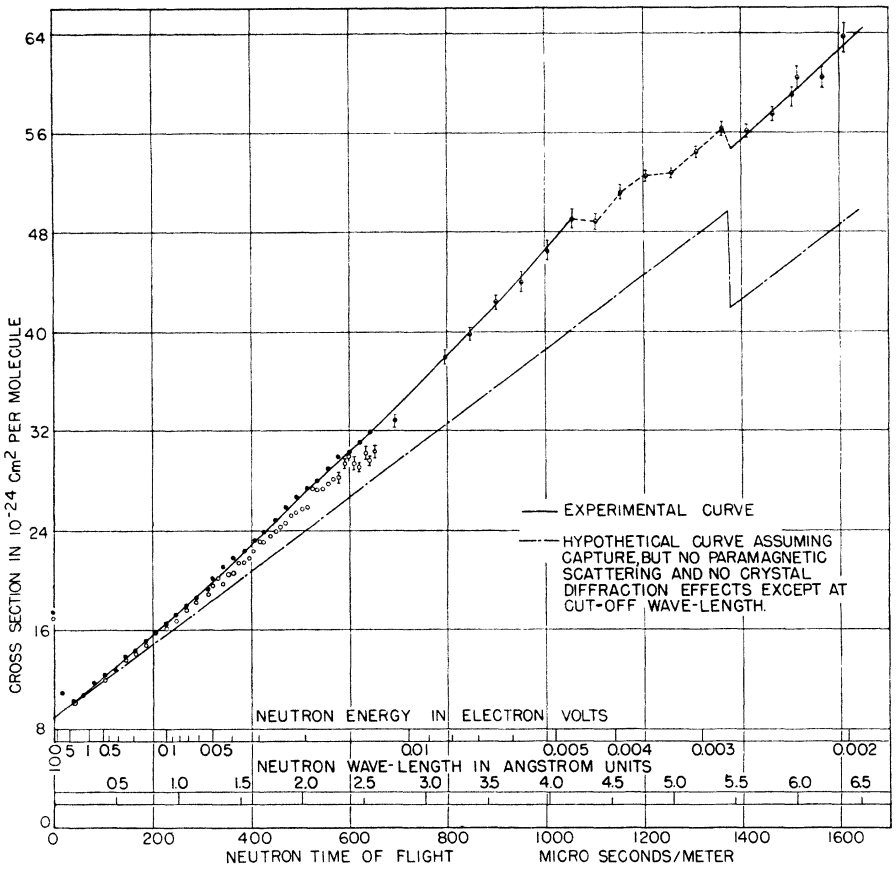

FIG. 8. The observed slow neutron total cross section of manganese fluoride compared with a hypothetical curve which neglects paramagnetic scattering. ● and ○ points were obtained with and without standard filters, respectively, with 11.13 g/cm² sample; ◒ points indicate 5.63 g/cm² sample.

is, however, over-simplified. Paramagnetic scattering is not spherically symmetrical as was assumed, but is instead under attainable conditions weighted in the forward direction. As a consequence, the error given by Eq. (2) is too low and must be corrected. The magnitude of the correction depends upon the wave-length of the incident neutrons; for short wave-lengths the angular dependence of scattering is large, while in the limit of very long wave-lengths (when the form factor becomes equal to unity) the scattering is spherically symmetrical.

Since the solid angle subtended by the detector at the sample is so very small, the differential form factor for scattering into the detector may be taken to be unity. It is assumed that the scattering is all single scattering, an assumption which leads to an upper limit for the in-scattering error. Since the mean free path of neutrons for paramagnetic scattering in the samples used (5 cm) is approximately equal to the maximum sample dimension, the effect of multiple scattering may be taken to be negligibly small on the basis of Melkonian's detailed analysis[22] of multiple scattering. The corrected relative error in cross section at a particular neutron wave-length may hence be represented by

$$\frac{\Delta\sigma_{\rm pm}}{\sigma_{\rm pm}}=\beta\frac{(1-T)}{T\ln T}\cdot\frac{1}{F} \qquad (3)$$

where F is evaluated at this wave-length. Taking $r_0=0.8$A as an approximate value, the correction factor $1/F$ has been calculated from the elastic form factor curve[10] for various wave-lengths. The results are summarized by Fig. 6, in which the maximum error, $\Delta\sigma_{\rm pm}/\sigma_{\rm pm}$, given by Eq. (3) (with $\beta=0.0006$ and

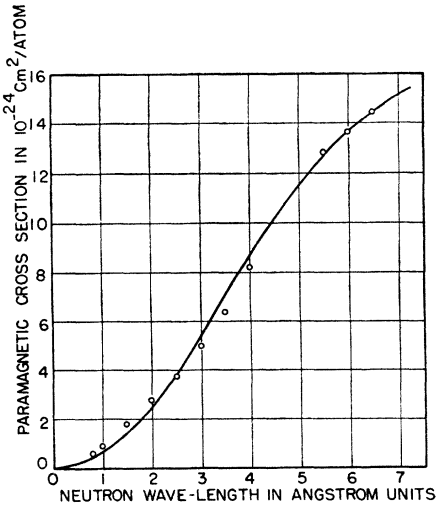

FIG. 9. Experimental values of $\sigma_{\rm pm}$ for Mn^{++} in manganous fluoride compared with a theoretical curve based on elastic scattering with $r_0=0.64$.

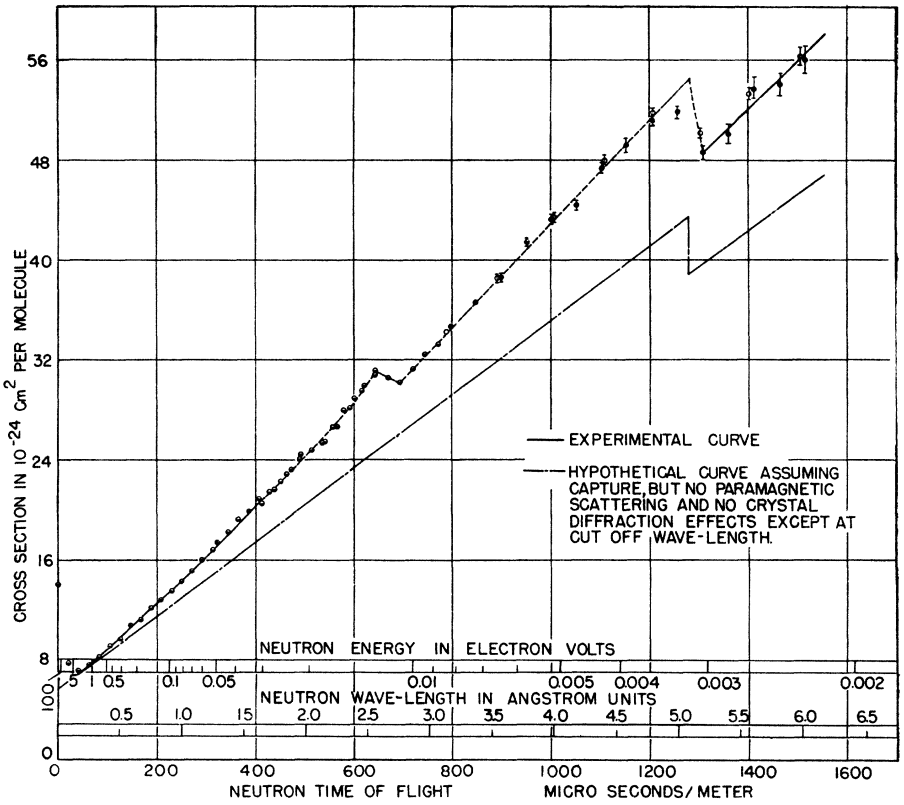

FIG. 10. The observed slow neutron total cross section of 7.25 g/cm² of manganous oxide compared with a hypothetical curve which neglects paramagnetic scattering. ◒ points were obtained with standard filters; ● and ○ points indicate 256 and 512 μsec. detection intervals, respectively.

$T=0.65$) is plotted as a function of neutron wavelength.

It should be mentioned at this point that the scattering in general has been tacitly assumed to be perfectly elastic, in the sense that the velocity of the scattered neutrons is the same as that of the incident neutrons. Under this restriction, the BF_3 counters, whose detection efficiency obeys a $1/v$ law, will count scattered and transmitted neutrons with the same efficiency. Moreover, only in the case of elastic scattering may the form factor in the forward direction be taken to be unity, and the use of Halpern's form factor be justified.

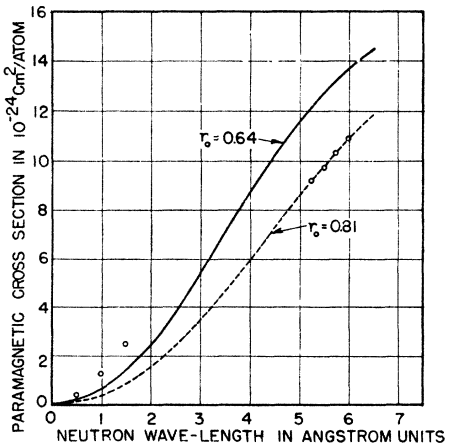

FIG. 11. Experimental values of σ_{pm} for Mn^{++} in manganous oxide compared with two theoretical curves based on elastic scattering.

Case II: 5-meter neutron path. The poorer geometry in this case leads to somewhat greater errors. The maximum total error as a function of λ is given in Fig. 6 (with $\beta=0.002$ and $T=0.65$). No corrections are given for $\lambda<3$A, since the 5-meter collimation was used only for $\lambda>3$A.

2. Sample Purity

Chemical analysis established the major composition of each sample, while spectrographic analysis showed the absence in any significant amount of high cross-section elements as impurities. However, the presence in any of the samples of about 0.1 percent by weight of hydrogen, a quantity difficulty to detect chemically, would introduce a serious error. This powerful effect of hydrogen arises from its very low atomic weight, high scattering cross section, and large reduced mass effect which makes the completely bound cross section four times as large as its free scattering cross section. Moreover, the hydrogen scattering is almost all incoherent and hence does not disappear at the cut-off wave-length for Bragg reflections. A simple calculation shows that the presence of 0.1 percent by weight of hydrogen in the manganous fluoride sample would lead to an error of +1.9 barns in the free scattering cross section of manganous fluoride; at low neutron energies (~0.002 ev) the error would increase because

of the reduced mass effect to a value between +3.4 and +7.6 barns, depending upon the form in which the hydrogen is bound. The error would then be comparable to σ_{pm}.

The manganese analyses indicate the absence of as much as 0.1 percent by weight of hydrogen *as water* (0.9 percent by weight of water), but do not preclude the presence of this quantity of hydrogen in elemental form. However, proof of the absence of appreciable quantities of hydrogen in any form can be obtained directly from the neutron transmission data. The intercept, obtained by extrapolating to high energy the hypothetical curve (where it merges with the experimental curve, i.e., at energies greater than 1 ev) represents the free scattering cross section of the molecule, σ_f, which is equal to the sum of the σ_f of the constituent elements. Thus, in the case of manganous oxide, the observed intercept is 5.6±0.2 barns, while the calculated sum is 5.5±0.1 barns. It may, therefore, be concluded that hydrogen, if at all present in the sample, contributes no more than 0.4 barn at neutron energies greater than 1 ev, with this error increasing because of the change in effective reduced mass of the hydrogen to a maximum of approximately 1.6 barns for very low neutron energies. Similar calculations for all the samples indicate the absence of large quantities of hydrogen.

3. Sample Thickness

The determination of the thickness of a sample in g per cm^2 involves measurements of the volume and thickness of the sample holder, and the weight of the sample. The errors in weighing and volume determination are negligible, being less than 0.1 percent. The sample holders were machined to tolerances which would give a maximum error of only 0.1 percent in the distance between walls. The accuracy of the machine work was checked by comparing the observed and calculated volumes of several sample holders.

4. Counting

a. *Statistical Accuracy*

The fractional uncertainty in the observed cross section is given by reference 22:

$$\frac{\Delta\sigma}{\sigma}=\frac{(1/N_i+1/N_0)^{\frac{1}{2}}}{\ln T}, \tag{4}$$

where N_i and N_0 represent the number of counts in the sample in and out positions, respectively, for the same number of neutron monitor counts. Whenever possible the sample thickness was adjusted to give a transmission within or close to 0.05 to 0.2, since the statistical error is a fairly constant minimum in this region. The statistical uncertainty is represented by vertical bars through the experimental points on the various cross section curves.

b. *Rate Dependence of Neutron Counters*

Figure 8 shows the cross-section data for manganous fluoride in the neutron wave-length region of 0 to 2.6A, obtained with and without the use of standard filters. Errors up to about 3 percent in the direction of decreased cross section are seen to be introduced when standard filters are not used. The good agreement between channels and the reproducibility of results resulting from the use of standard filters, as well as theoretical considerations, indicate that rate dependence errors have been effectively eliminated.

5. Change in Reduced Mass

Because the effective reduced mass of an atom changes with the binding, the cross section of an atom completely bound in a crystal is larger than the free cross section of this same atom by the factor $[(A+1)/A]^2$, where A is the atomic weight. The magnitude of this effect is shown in Table I, which gives the difference in the bound and free cross section for each sample, neglecting capture, paramagnetic scattering, etc. If the form factor for the binding was known, then corrections could be made for the increase in cross section with neutron wave-length. Unfortunately, the binding is a complicated phenomenon which is not now well known. However, for neutron wave-lengths beyond λ_c all but a small part of the nuclear scattering disappears. Any error due to change in reduced mass is then present only in the small residual incoherent scattering cross section, and is, indeed, only equal to a small part of the latter. It may be concluded then that for wave-lengths smaller than λ_c, errors up to the maximums shown in Table I are incurred, but that beyond λ_c the error due to changed reduced mass is negligible. The errors will tend to make the calculated σ_{pm} larger than its true value.

6. Effect of Resolution Width

The effect of varying neutron intensity and transmission with neutron energy may be considered to change the effective weighting over the resolution function so as to cause the correct transmission to be observed for a slightly different time of flight value. For detection interval widths of 512 μsec. (or greater) the shift was found to be significant enough to warrent correction. The method described by Rainwater and Havens[19] was used.

7. Stray Neutrons

The error introduced by stray neutrons is considered to have been made negligibly small by the methods already described.

8. Separation of Paramagnetic Scattering from Nuclear Scattering

For those wave-lengths below λ_c at which there are no perturbing crystal diffraction effects, the method of

subtracting the hypothetical from the experimental curve is probably accurate to within ± 0.5 barn. This probable error is attributed to the uncertainty in the plotting of these curves, and to the possible presence of unresolved diffraction peaks. Beyond the cut-off the approximation of the residual incoherent scattering cross section introduces a further uncertainty in σ_{pm} of $\sim\pm 0.75$ barn.

9. Summary

Since the determinate errors discussed above are generally much smaller than the known indeterminate errors, no corrections other than for background and time of flight shift were applied to the observed results. For $\lambda<\lambda_c$ the maximum error may be taken to be $\sim\pm 0.5$ barn, while beyond λ_c the maximum error is probably $\sim\pm 1.5$ barns.

DISCUSSION OF RESULTS

In order to determine accurately σ_{pm} for MnF_2 and MnO by the method already described, it is necessary to have an accurate value of the capture slope of manganese. A slow neutron transmission study of 16.92 g/cm² of pure manganese was therefore carried out. The results are shown in Fig. 7. The best $1/v$ line is given by the equation

$$\sigma=(1.80\pm 0.05)+(2.14\pm 0.02)E^{-\frac{1}{2}}.$$

This may be compared with the recently published value[24]

$$\sigma=(2.2\pm 0.4)+(2.24\pm 0.05)E^{-\frac{1}{2}}.$$

The new value is considered to be more accurate because of the use of standard filters, and the particular care taken to remove hydrogen from the sample.[26]

Large values of σ_{pm} for manganous fluoride were found at $\lambda>\lambda_c$, as shown in Fig. 8. No analysis of the experimental curve was made between 4 and 5.5A because of the perturbing effect of crystal diffraction peaks. In constructing the hypothetical curve only the capture slope of manganese was taken into account, since the capture of fluorine is very small.[27] The differ-

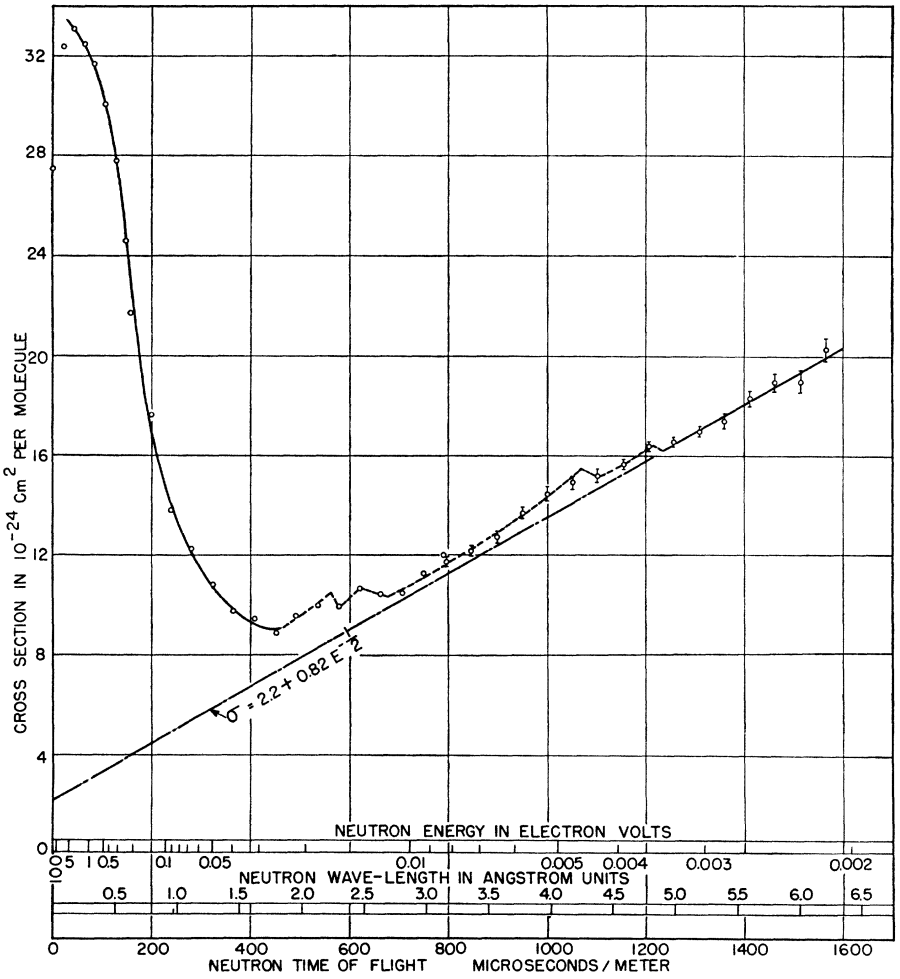

FIG. 12. The observed slow neutron total cross section of 19.30 g/cm² of α-ferric oxide.

[26] Potter, Hayes, and Lukens, Am. Inst. of Mining and Met. Eng., Tech. Pub. No. 1809 (1945). These investigators have shown that considerable quantities of hydrogen are adsorbed or entrapped in electrolytic manganese.

[27] Manley, Haworth, and Luebke, Phys. Rev. **59**, 109 (1941); H. Volz, Zeits. f. Physik **121**, 201 (1943); C. O. Muehlhause and M. Goldhaber, Phys. Rev. **70**, 85 (1946).

ence between the experimental curve and the hypothetical curve beyond λ_c is attributed to paramagnetic scattering.

In Fig. 9 the experimental values of σ_{pm} for MnF_2 are compared with a theoretical curve based on the Halpern-Johnson elastic form factor. The parameter r_0 was taken to be 0.64A to give the best fit. It is perhaps of interest to compare this value of r_0 with the empirical ionic radius of Mn^{++} in crystals as given by Pauling,[28] namely 0.80A. Even though MnF_2 is not expected to have a large degree of spin coupling, since Δ is only 113, the agreement between the experimental points and the theoretical curve is surprisingly good. These results for MnF_2 represent an improvement over the preliminary results already reported[10] in that standard filters and a more accurate manganese capture slope were used.

Similar results for MnO are shown in Figs. 10 and 11. It is to be noted that beyond the cut-off σ_{pm} is considerably less than for MnF_2 at corresponding values of λ. This can be attributed to the large spin coupling in MnO. The dashed curve in Fig. 11 was constructed by taking the parameter r_0 to be 0.81A so as to fit the experimental points beyond λ_c. The agreement between the experimental points and this theoretical curve is poor at short wave-lengths, a result to be expected if there is considerable inelastic scattering in virtue of spin coupling. For, it then becomes rather meaningless to fit a theoretical curve based on an *elastic* form factor to the experimental results. It is more reasonable to compare the experimental results with the same theoretical curve ($r_0=0.64$A) with which the MnF_2 results agree so well, particularly since coupling should not appreciably change r_0. Such a comparison may be made with the solid curve in Fig. 11. It is seen that σ_{pm} falls well below the solid theoretical curve at long wave-lengths. This is explicable on the basis that inelastic scattering causes a greater attenuation of F the longer is the neutron wave-length. In the limit of long wave-lengths inelastic collisions become energetically impossible when the energy change involved, $h\nu$, is greater than the neutron energy, while hyperelastic collisions are greatly restricted by the Boltzmann factor when $h\nu > kT$.

The α-ferric oxide results can best be discussed in the light of the magnetic properties of this substance. A recent careful study by Hayes[29] shows that although the susceptibility values of α-Fe_2O_3 are those of a strongly paramagnetic substance, it displays properties of incipient ferromagnetism. It was found to have a slight residual magnetism and a Curie point (685°C), and to exhibit hysteresis phenomena. A very large degree of spin coupling is hence expected to be present in this compound. Since Fe^{+++} has five unpaired $3d$ electrons, Eq. (1) predicts the same amount of paramagnetic scattering for it as for Mn^{++}. Figure 12 shows the observed dependence of the total cross section on neutron energy for α-Fe_2O_3. The latter was oriented in the collimating system so that the neutron beam was parallel to the three-fold symmetry axis of the crystal.[30] As is typical of large single crystals,[14] the cross section decreases rapidly with increasing neutron wave-length. At 3A almost all the coherent scattering has vanished, and a straight line drawn through the remaining points and extrapolated back to zero wave-length fits the equation $\sigma=2.2+0.82E^{-\frac{1}{2}}$. Recent unpublished measurements in this Laboratory for pure iron give a $1/v$ slope of 0.41 per iron atom. Since a considerable part of the 2.2-barns residual cross section must be attributed to spin, thermal, etc., effects (see Table I), it is concluded that very little, or no paramagnetic scattering occurs. This is not a surprising result for a paramagnetic substance in which spin coupling is so strong that it displays weak ferromagnetism.

Experiments of the kind discussed in this paper, complemented, perhaps, by angular scattering experiments (which can reveal the differential form factor for paramagnetic scattering), offer a new tool for investigating paramagnetism.

ACKNOWLEDGMENT

The author wishes to express his appreciation to Professors T. I. Taylor, W. W. Havens, Jr., L. J. Rainwater, and J. R. Dunning for help and guidance in the work, to Professor O. Halpern for his interest and criticism, and to the members of the Columbia cyclotron staff, particularly Miss M. Levin, for assistance in the measurements. He is also indebted to the AEC for the support which made this research possible.

[28] L. Pauling, *The Nature of the Chemical Bond* (Cornell University Press, Ithaca, 1940), second edition, p. 350.

[29] E. T. Hayes, Bur. of Mines Report of Investigations 3570, June, 1941.

[30] In this position the most widely spaced plane which can reflect, the 111 plane, is perpendicular to the neutron beam. Reflection from this plane then takes place at $\lambda=9.14$A, which is the same cut-off as for a microcrystalline sample.